Fluid exciting force due to flutter and rotor-stator interactions in axial flow turbines

IOP Conf. Series: Earth and Environmental Science **240** (2019) 022061 doi:10.1088/1755-1315/240/2/022061

Fluid exciting force due to flutter and rotor-stator interactions in axial flow turbines

K Ajiro[1], K Matsuda[1], K Onishi[1], T Mineshima[1], and K Miyagawa[2]

[1] Department of Applied Mechanics, Waseda University, Tokyo, 1690072, Japan
[2] Department of Applied Mechanics and Aerospace Engineering, Waseda University, Tokyo, 1690072, Japan

kazushi.0727@asagi.waseda.jp

Abstract. In recent years, the size and the speed of axial flow type hydraulic turbines have been continuously increased, leading to an increase of the fluid exciting forces due to rotor-stator interactions in hydraulic machines featuring both rotor and stator. In addition, the use of composite material for the blades of large hydraulic machines is increasingly investigated. Such flexible and lightweight hydrofoils can however easily experience self-excited vibration such as flutter effect. Fluid exciting forces generated in hydraulic machines might cause resonance, fatigue of the blade and finally damage. This paper aims to evaluate fluid exciting forces produced by rotor-stator interactions in axial flow turbines and the hydro-elastic response to the flutter of a flexible hydrofoil. To evaluate fluid exciting forces due to rotor-stator interactions, experiments are carried out using a closed-loop water channel featuring an axial flow turbine. The pressure distribution on the blade surface and the influence of axial distance between rotor and stator on the pressure fluctuations amplitude on the blade surface are investigated. A good agreement between experimental and numerical values is found. Regarding the flutter effect, FSI (Fluid Structure Interaction) simulation of one hydrofoil coupling RANS (Reynolds-averaged Navier–Stokes equations) and FEM (Finite Element Method) simulation is carried out to study the three-dimensional behaviour of the flutter.

Keywords: fluid exciting force, blades interactions, axial flow turbine, flutter, hydrofoil.

1. Introduction

In recent years, the size and the speed of axial flow type hydraulic turbines have been continuously increased. As a result, the fluid exciting forces due to rotor-stator interactions tend to increase in hydraulic machines featuring both rotor and stator. Moreover, the use of composite material such as CFRP (Carbon Fiber Reinforced Plastics) and GFRP (Glass Fiber Reinforced Plastics) for the turbine blades of large hydraulic machines is now in the spotlight. Blades made of such material are more flexible and lighter and can easily experience self-excited vibration such as flutter effect. Fluid exciting forces generated in hydraulic machines might cause resonance, blade fatigue and damage. Therefore, methodologies to predict vibration phenomena such as rotor-stator interactions and excitation dynamics such as flutter are required for the design stage of hydraulic machines.

Concerning the investigation of rotor-stator interaction, Kemp et al. [1] derived the theoretical amplitude of potential interactions and wake flow interactions by studying a simple model of a rotor and stator blades row. Recently, Funazaki et al. [2] performed experimental investigations on a reduced scale model of an axial flow turbine including measurements of the velocity, total pressure and static pressure

distribution on the stator blades. Time average velocity, flow angle and total pressure distribution on the rotor blade outlet were also measured by means of a Pitot tube. They observed fluctuations of the entropy distribution between rotor and stator blade rows caused by rotor-stator interaction. However, in hydraulic turbines, studies evaluating the fluid exciting forces due to blades interaction and the impact of design parameters modification are not sufficient.

Concerning the flutter effect of hydrofoils, Besch et al. [3] conducted experimental studies on two-dimensional flexible hydrofoils and used theoretical equations to establish stability limits. In recent years, Spentzos et al. [4] studied the behaviour of separation vortices developing on the upper surface of 3D NACA blade by performing Computational Fluid Dynamics (CFD) with respect to Dynamic Stall, which is the cause of stall flutter. Chae et al. [5] conducted tests on flexible hydrofoils and evaluated the vibration behaviour of flutter by performing Fluid Structure Interaction (FSI) simulation including rigidity and damping coefficients for the structural part similar to the ones of a 2D rigid body. However, researches focusing on hydrofoil flutter with 3D FSI simulation and prediction method of stability limit of flutter with arbitrary shape blade are not sufficient.

This paper aims to fulfil this gap by evaluating the fluid exciting force induced by rotor-stator interactions on axial flow type hydraulic turbine and studying the hydro-elastic response to the flutter of a flexible hydrofoil.

2. Experimental setup

2.1. Hydro turbine

An overview of the test apparatus is shown in figure 1. It consists in a closed-loop water channel featuring two test sections, a cavitation tunnel for tests on hydrofoils and a hydro turbine for tests on axial flow turbines. The flow rate is adjusted by using two centrifugal pumps connected in parallel. The rotational speed is controlled with an inverter.

An enlarged view of the hydro turbine test section is shown in figure 2. The maximum flow velocity is 4 m/s and the rotor rotation speed can be varied from 600 to 1200 rpm. In addition, the axial spacing between the rotor and the stator can be varied by steps of about 5% of the rotor diameter D by using spacers. A motor is connected to the shaft of the rotor via a pulley.

The rotor features MEL009 hydrofoil type. The tip clearance is 0.5 mm. A small pressure sensor is attached to the rotor blade pressure side at midspan. In addition, the force generated on the rotor blade can be measured by strain gauges installed at the blade root. The stator blades are NACA0012 hydrofoil type, which can induce swirling flow. The tip clearance is also 0.5 mm. The parameters of the axial turbine are given in Table 1.

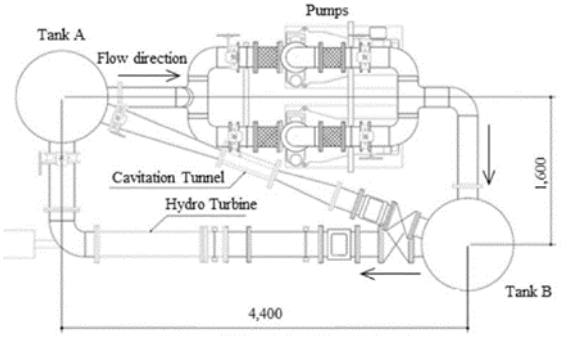

Figure 1. Overview of the test apparatus.

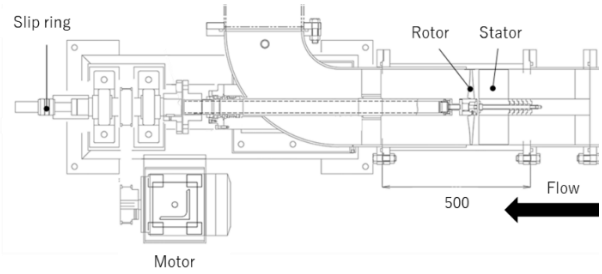

Figure 2. Enlarged view of the axial turbine.

Table 1. Detailed parameters of axial turbine.

Items	Values	Units
Number of stator blades *Zs*	8	-
Number of rotor blades *Zr*	5	-
Rotor tip diameter *D*	0.2534	m
Design point tip speed ratio *TSR*	3.67	-
Design point flow rate *Q*	0.165	m^3/s
Rotational speed	1064	rpm
Axial distance between rotor and stator *d/D*	0.0668 - 0.362	-

In addition, several parameters are measured, including:

- flow rate by using an electromagnetic flowmeter;
- forces generated on the blade and shaft torque by using strain gauges;
- differential pressure across hydro turbine by a differential pressure transducer;
- blade surface pressure;
- number of rotations by a noncontact type tachometer;
- wall static pressure by small pressure transducers.

The signals from the rotating part is transmitted to the stationary system by a slip ring. Each measurement is recorded by a universal recorder (EDX-200A).

2.2. Cavitation tunnel

Investigation of the flutter effect are performed in the cavitation tunnel. It is made of acrylic to visualize hydrofoil and has a 100 mm × 100 mm cross section. The maximum flow velocity is 15 m/s. The test section and the hydrofoil are shown in figure 3. The chord length and span of the hydrofoil are 24 mm and 95 mm, respectively. It is made of acrylic. A weight made of A6061 is placed at the tip of the hydrofoil to change its eigenvalues. Pressure is measured upstream and downstream of the test section (sensors P1 and P4 in figure 3a). In addition, the hydrofoil vibrations are measured by strain gauges attached to the hydrofoil root. By using strain gauges located at both the leading and trailing edges of the hydrofoil, both torsion and bending modes can be highlighted.

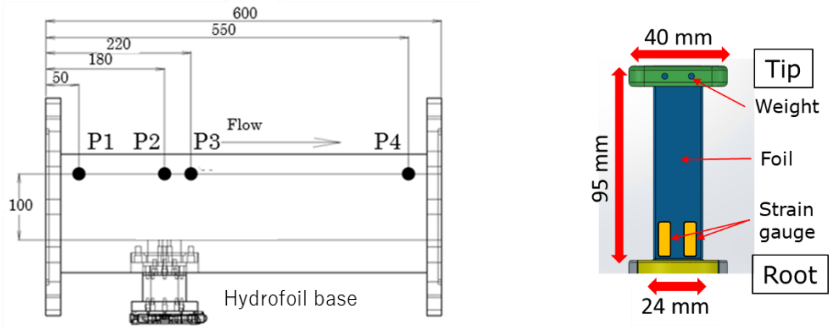

a. Enlarged view. **b.** Sketch of the hydrofoil.

Figure 3. Sketch of the cavitation tunnel.

3. Rotor-Stator Interactions

3.1. Simulation set-up

Flow in the axial turbine is investigated by CFD simulation with the commercial software ANSYS CFX 17.2. URANS (Unsteady Reynolds-Averaged Navier-Stokes equation) simulations using the SST k-ω (Shear Stress Transport) turbulence model are carried out to evaluate the time history of pressure and force on the rotor blades induced by rotor-stator interaction. According to Iino et al [6,7], the SST k-ω turbulence model is suitable for prediction of the flow near the blade surface of pumps and turbines.

The simulation domain is shown in figure 4. The model includes both rotor and stator, the struts used to hold rotor and stator and a L-shaped elbow located at rotor outlet.

The meshing is mainly made of tetrahedra elements. Near the wall surface, prism layer meshing is used to simulate the boundary layer. The CFD conditions are summarized in Table 2. The created meshing is shown in figure 5. Information on the meshing is given in Table 3. The influence of gravity is not considered in this simulation.

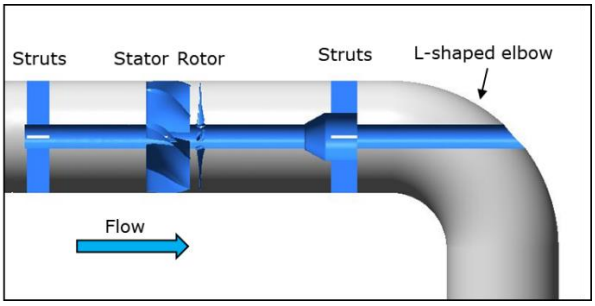

Figure 4. View of CFD domains.

Table 2. CFD conditions.

Place	Values
Inlet (kg/s)	Mass flow average 164.82
Outlet (Pa)	Static pressure 0
Wall	No slip (Counter rotating wall)
Blades	No slip
Strut	No slip
Time step (s)	4.31E-5

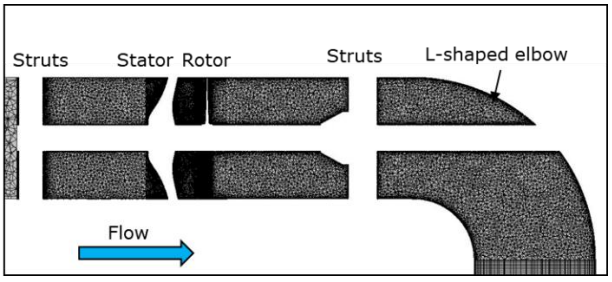

Figure 5. Meshing configuration.

Table 3. Meshing details.

Flow domains	Nodes (k)	y^+
Rotor	5212	2.5
Stator	3526	2.5
Strut	1549	10
Total	1193E+1	-

3.2. Experimental results

In this section, the experimental results are presented. figure 6 shows the time history of the pressure fluctuation coefficient C_p on the rotor blade during one revolution T of the rotor (axial distance d/D= 0.067*)*. C_p is expressed by the following equation:

$$C_p = P/(\frac{1}{2}\rho U^2) \quad (1)$$

where P is the pressure, ρ is density and U is the inlet flow velocity. figure 7 shows the FFT (Fast Fourier Transform) of the raw pressure fluctuations. The frequency f is made dimensionless by the rotor rotational frequency N.

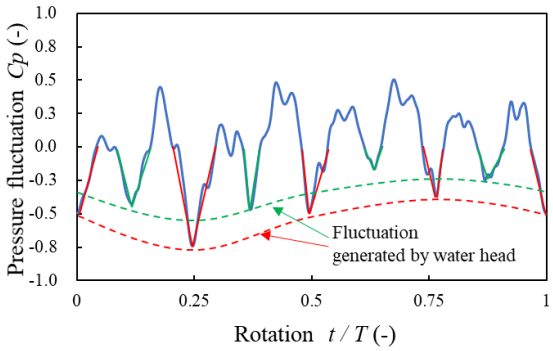

Figure 6. Pressure fluctuation coefficient on the blade surface.

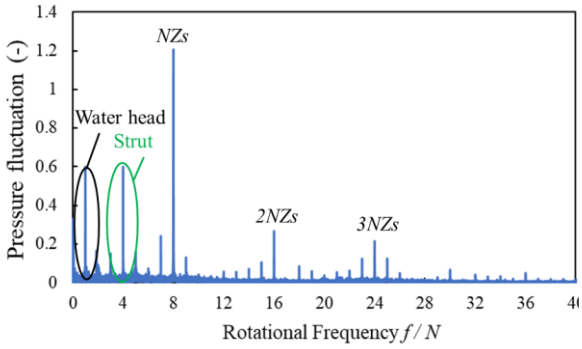

Figure 7. Result of FFT.

In addition to the fluctuations generated by the water head at a frequency equal to the rotor rotation frequency, two kinds of fluctuations for which low-pressure peak occur four times per rotor rotation are observed, see red and green peaks in figure 6. These pressure peaks are almost equally spaced and forms all together pressure fluctuations featuring 8 cycles during one rotor rotation.

In figure 7, peaks at $f/N = 1$, 4, 8, 16 and 24 are dominant. The one at the rotor frequency might be caused by the change of the water depth due to the rotor rotation. Since the number of stator blades is equal to $Zs = 8$, the frequencies $f/N = 8$, 16 and 24 correspond to multiples of NZs. Fluctuations at these frequencies are therefore induced by the interaction between the rotor and the stator. In addition, the fluctuations at $f/N = 4$ might be induced by the interaction of the rotor with the struts, since the number of struts is equal to 4.

Generally, the blade rows interactions are classified into two types of interactions, the potential interaction and the blade wake interaction. The peak induced by potential interaction is at the NZ component (with Z the number of blades of the influencing blade row) and the ones induced by blade wake interaction are at the nNZ components (with $n = 1, 2, 3...$). In figure 7, it is found that the rotor blades are subject to both potential interaction and blade wake interaction with stator and the strut.

From the above, the stator blade alternately has blades which interfere with the downstream strut (green peaks in figure 6) and blades which do not interfere (red peaks in figure 6), since the peaks are different in the waveform of figure 6.

3.3. Validation of computational results

In this section, the results of the CFD are validated by comparison with experimental results. figure 8 compares the simulated pressure fluctuations with the measured ones. In figure 8, the average value of the pressure fluctuations is set at 0. In addition, a comparison of the FFT peaks is shown in figure 9.

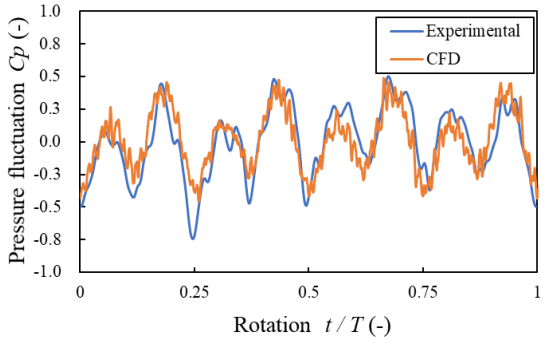

Figure 8. Comparison of pressure fluctuations.

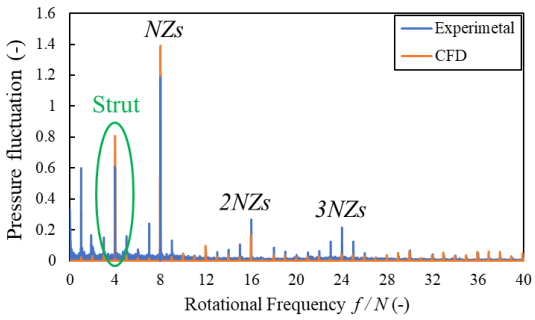

Figure 9. Comparison of FFT peaks.

As shown in figure 8, a very good agreement between experiments and simulations is found even if the gravity is not considered in the simulation. In general, the shape of the pressure fluctuations is well-reproduced by the simulation, with however a slight discrepancy in terms of amplitude. Moreover, as shown in figure 9, CFD results of the amplitude at the frequencies *NZs* is larger than the experimental ones whereas CFD results at the frequency *2NZs* and *3NZs* are smaller. Therefore, the present numerical simulation overestimates the potential interactions and underestimates the blade wake interactions of the front stator. Interactions between the strut and the rotor is also reproduced by the simulation but the level is overestimated.

Attention is paid to the pressure fluctuations at the frequency equal to *NZs*. The influence of the axial distance between rotor and stator on the amplitude of pressure fluctuations at this frequency is investigated. A comparison between simulations and experiments is shown in figure 10.

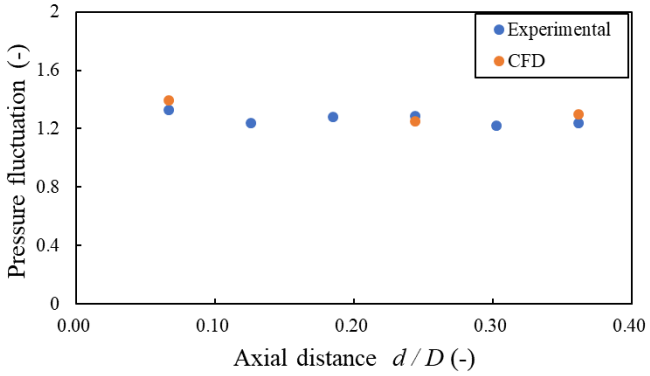

Figure 10. FFT amplitude of pressure fluctuations at the frequency equal to *NZs*.

As shown in figure 10, the amplitude of pressure fluctuations is almost not affected by the axial distance *d/D* for the range of investigated values. Moreover, a very good agreement is found between experimental and numerical results. The interaction between the rotor and stator can be fairly reproduced by CFD for any axial distance between rotor and stator.

4. Flutter

4.1. FSI simulation

Concerning the flutter effect, FSI simulation is carried out by combining 3D CFD and 3D FEM simulation. The simulation conditions are shown in Table 4. Physical properties of the materials used for the simulation of solid regions are shown in Table 5-6.

Table 4. FSI simulation conditions.

Items	Setting condition
General-purpose code	STAR-CCM+ 12.04.011
Calculus of finite differences	Implicit method
Solver	Discrete type
Turbulence model	SST k-ω
Material law	Isotropic linear elasticity
Fluid region deformation	Mesh morphing
Solid region deformation	Solid stress
Data movement method (Fluid to Solid)	Pressure / Traction
Data movement method (Solid to Fluid)	Displacement

Table 5. Physical parameters of Acrylic.

Items	Values
Density (kg/m^3)	1145.0
Young's modulus (Pa)	3.3E+9
Poisson's ratio	0.45

Table 6. Physical parameters of A6061.

Items	Values
Density (kg/m^3)	2680.0
Young's modulus (Pa)	7.06E+10
Poisson's ratio	0.33

The results of FSI simulation with an attack of angle (AOA) 0 degree (two-degree-of-freedom flutter) are shown in the next sections. The flow conditions are given in Table 7. The joint surface between the hydrofoil portion and the tip portion is simulated as complete fixation.

The meshing used for the simulation is shown in figure 11. The meshing is generated by polyhedral and prism elements in the fluid region whereas the solid region is generated by tetra and prism elements. The upper limit of the Y^+-value is set at 100 and 10 for the wall and hydrofoil surfaces, respectively.

Table 7. FSI simulation conditions.

Items		Setting condition
AOA (degree)		0
Inlet (m/s)		Velocity 5
Outlet (Pa)		Static pressure 0
Foil material		Acrylic
Weight material		A6061
Time step (second)		0.0001
Mesh nodes	Fluid (k)	2889
	Solid (k)	41.25

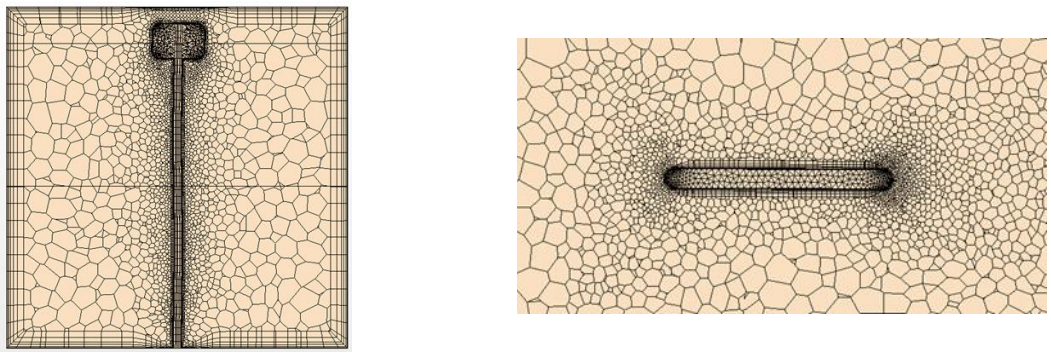

Figure 11. Meshing configuration.

4.2. Experimental results

In this section, experimental results are presented. The FFT of the time history signals of torsion and bending strain are shown in figure 12 for a wide range of velocity under the form of a waterfall diagram. The AOA is 0 degree for this case.

In figure 12a, the first peak corresponds to the first eigenmode of torsion, which was confirmed by the result of a modal analysis. In figure 12b, a peak corresponding to the first eigenmode of bending and a peak induced by Karman vortex shedding (St = 0.241) are observed. A resonance occurs when the Karman vortex frequency and the structure eigenvalue match.

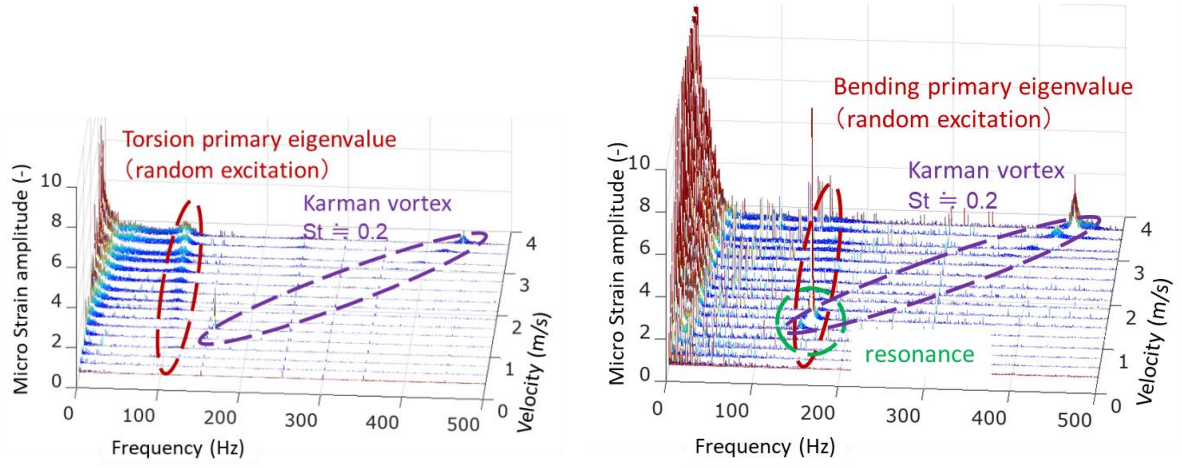

a. Torsion strain. **b.** Bending strain.

Figure 12. Waterfall diagram of FFT of strain measurements (AOA 0 degree).

Experimental results with AOA 8 degrees are shown in figure 13. Only frequencies up to 100 Hz are shown in this figure. Contrary to the case with AOA 0 degree, the frequencies of the torsion eigenvalue and bending eigenvalue match and a coupling between torsion and bending mode might occur. Therefore, it turned out that the flutter can occur in these conditions. In addition, depending on the AOA, stall flutter might also appear.

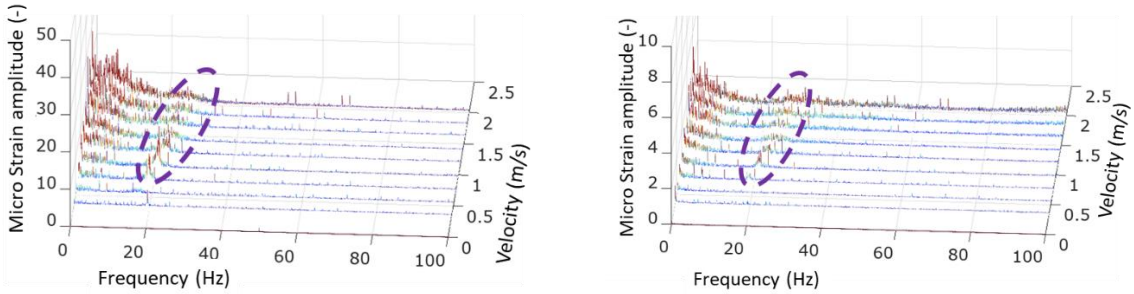

a. Torsion strain. **b.** Bending strain.

Figure 13. Waterfall diagram (AOA 8 degree).

4.3. Computational results

It is confirmed by the FSI simulation that vibrations of the blade in the form of limit cycles are generated. In addition, it is also confirmed by FFT that the vibration frequency is equal to 482.2 Hz. figure 14a shows the simulated displacement contour of the hydrofoil and figure 14b shows the contour of the turbulent energy in the centre cross section in the span direction.

Structural eigenvalues obtained by eigenvalue analysis without attenuation are 17.7 Hz for the primary bending mode, 84.8 Hz for the primary torsion mode and 259.6 Hz for the secondary bending mode. Moreover, the vibration frequency obtained by FSI simulation is very high compared with the structural eigenvalue. Based on figure 14a, the tendency of the hydrofoil to vibrate in a mode for which the hydrofoil tip is a node can be confirmed. In the real eigenvalue analysis, the tip of the hydrofoil vibrates as a node, but the reason why it become a belly in FSI simulation is that the tip weight has a very large inertial mass. Since the real eigenvalue analysis does not actually vibrate the object, it cannot consider the effect of such inertial mass. For this reason, real eigenvalue analysis is performed a second time with the foil tip simply supported as boundary condition (only angular displacement is allowed).

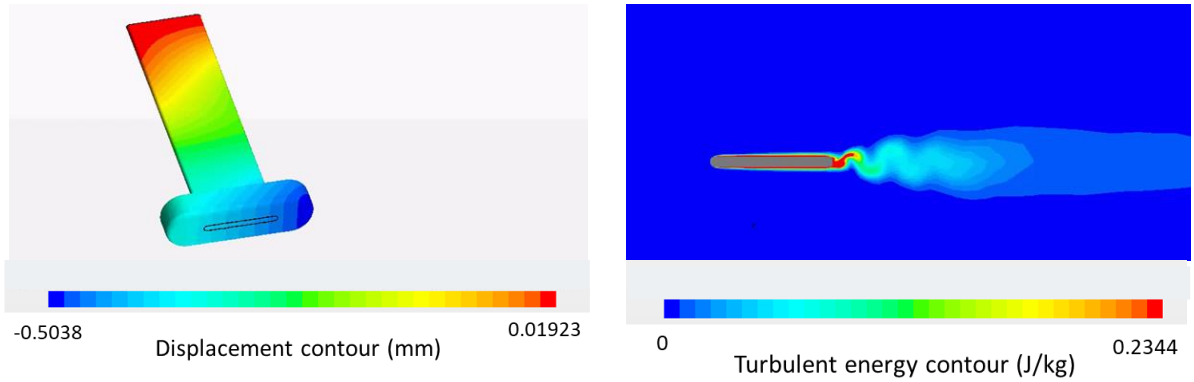

a. Displacement contour. **b.** Turbulent energy contour.

Figure 14. Results of FSI simulation (AOA 0 degree).

Modal analysis results are shown in Table 8. According to these results, it is confirmed that although the torsional eigenvalues hardly change, the bending eigenvalues are greatly increased. In addition, based on the comparison with the FSI simulation results, the tendency of the hydrofoil to vibrate in the second bending mode is confirmed. It is assumed that the vibration frequency of the FSI simulation is low due to the additional mass effect induced by the fluid around the test hydrofoil.

Table 8. Results of modal analysis.

Items	Results frequency (Hz)
Primary bend	84.73
Primary torsion	218.4
Secondary bend	648.7
Secondary torsion	1158.9

The case of AOA 8 degree is now investigated. The conditions of the simulation are shown in Table 9. Results obtained from FSI simulation are shown in figure 15.

Table 9. FSI simulation conditions.

Items		Setting condition
AOA (degree)		8
Inlet (m/s)		Velocity 3
Outlet (Pa)		Static pressure 0
Blade material		Acrylic
Weight material		A6061
Time step (second)		5.0E-5
Mesh nodes	Fluid (k)	2895
	Solid (k)	41.72

It is confirmed by figure 15 that the torsion vibrations dominate with AOA 8 degree. Moreover, the flow separates on the foil suction surface and periodic vortices shedding is observed. Since FFT is performed on the time history waveform of the displacement of the blade tip, it becomes clear that peaks exist at 19.4 Hz and 174.7 Hz. From the experimental results, it is found that a stall occurs at AOA 8

degree, so it is considered that stall flutter also occurs in FSI simulation. The flutter vibration at the AOA 0 degree and 8 is revealed by FSI simulation results.

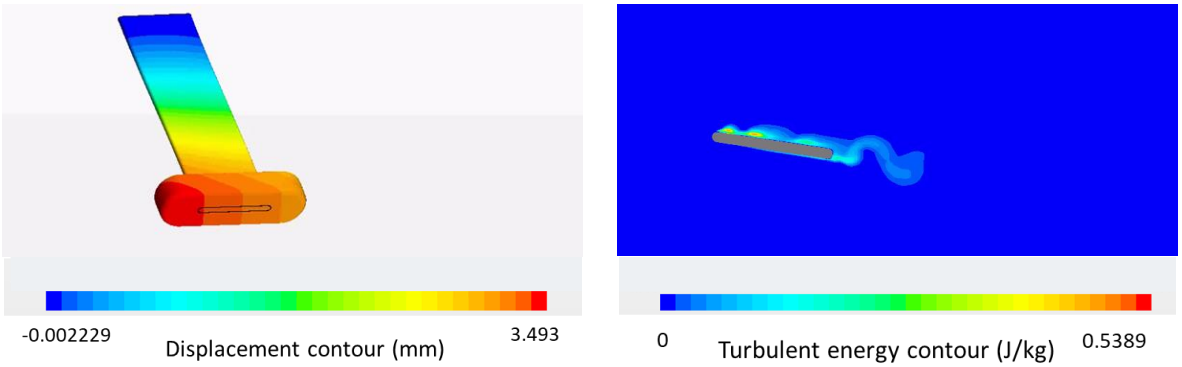

a. Displacement contour. **b.** Turbulent energy contour.

Figure 15. Results of FSI simulation (AOA 8 degree).

4.4. Validation of computational results

In the following, the FFT results of the measured and simulated vibration waveform are compared. The frequencies obtained by FSI simulation are summarized in Table 10. The experimental results are shown in Table 11.

Table 10. Results of FSI simulation.

AOA (degree)	Flow velocity (m/s)	Frequency (Hz)
0	5	177.7
		482.2
8	3	19.41
		174.8

Table 11. Experimental results.

AOA (degree)	Flow velocity (m/s)	Frequency (Hz)
0	3.68	159.2
		444.2
8	2.04	26.09
		164.7

Among frequency peaks with AOA 0 degree, the first peak corresponds to the first bending eigenmode. Experimental and simulation results show a good agreement in terms of value, even if the computational results are slightly higher. It might be induced by the underestimation of the added mass of the weight in the FSI simulation. The second peak is the frequency due to the Karman vortex as seen in figure 12. By FSI simulation, it is highlighted that the hydrofoil is excited by the Karman vortex. The Strouhal number is equal to 0.202 in the simulation and 0.241 in the experiments. Even if a slight discrepancy is observed, one can assume that the frequency of the Karman vortex shedding is well estimated by the simulation.

For the case with AOA of 8 degree, the first peak corresponds to the frequency of the flutter identified by the comparison of bending and torsion strain in figure 13. It is in relative good agreement

with FSI simulation results. The second peak corresponds to the first bending eigenmode and it can be confirmed that the FSI simulation result is higher than the experimental one, similarly to the case with AOA 0 degree.

Although the predicted vibration frequencies do not exactly match the experimental results, the results are qualitatively in a good agreement. In the experiment, the torsion first-order eigenvalue is lower than the bending first-order eigenvalue and the same tendency is observed in the modal analysis when the hydrofoil tip is simply supported. In addition, the experimental results show that the tip vibrates as a node. The same vibration mode appears also in the computational results with AOA

0 degree, which reveals that the results of FSI simulation are qualitatively in agreement with the experimental results.

5. Conclusions

(1) Based on the axial turbine experimental results, fluid exciting force acting on the rotor is influenced by the interactions with the stator blades.
(2) The URANS simulation results overestimate the influence of potential interaction compared with the experimental results, and it is found that the influence of the blade wake interaction is underestimated.
(3) It is found that the amplitude value of the pressure fluctuations on the rotor blade pressure surface does not change extremely even if the axial distance between rotor and stator increases.
(4) The results of the 3D Fluid-Structure-Interaction simulation of the stalled flutter have good agreement with the experiment results and both the vibration mode and the peak frequency of the hydrofoil can be predicted.

Acknowledgement

[1] The authors would like to thank the WISE (Waseda Research Institute for Science and Engineering) for providing support to the presented research, in context of the project: 'High performance and high reliability research for hydraulic turbomachinery systems'.
[2] This work was done as part of the project financially supported by the NEDO (New Energy and Industrial Technology Development Organization). We would like to thank the organizers of this work.

Reference

[1] N H Kemp and W R Sears 1953 Aerodynamic Interference Between Moving Blade Rows *Journal of The Aeronautical Sciences* ed Institute of the Aeronautical Sciences pp 585-597
[2] K Funazaki, K Yamada, M Kikuchi and H Sato 2010 Studies on Effects os Stator-Rotor Axial Gap on Aerodynamic Perfomance of a Single Stage Axial Turbine (Experiment and CFD) *Turbomachinery (Vol.38 No.6)* ed Turbomachinery Society of Japan pp 14-24
[3] P K Besch and Y-N Liu 1971 Flutter And Divergence Characteristics Of Four Low Mass Ratio Hydrofoils *Ship Performance Department Research And Development Report* ed Naval Ship Research and Development Center pp 1-51
[4] A Spentzos and G Barakos et al 2004 CFD Investigation of 2D and 3D Dynamic Stall *AHS 4th Decennial Specialist's Conference on Aeromechanics*
[5] E J Chae and D T Akcabay et al 2017 Influence of flow-induced bend-twist coupling *Journal of Fluids and Structures* ed Elsevier pp 323-340
[6] M Iino, K Tanaka, K Miyagawa and T Okubo 2003 Numerical analysis of 3d internal flow with unstable phenomena in a centrifugal pump *Proceedings of the 7th Asian International Conference on Fluid Machinery* pp 7-10
[7] M Iino, K Tanaka, K Miyagawa and T Okubo 2003 Numerical simulation of hysteresis on head/discharge characteristics of a centrifugal pump *Proceedings of the ASME FEDSM 4th ASME_JSME Joint Fluids Engineering Conference* pp 6-10